Available online at www.sciencedirect.com
ScienceDirect
Journal of the European Ceramic Society 30 (2010) 3331–3337
www.elsevier.com/locate/jeurceramsoc

Densification of transparent yttrium aluminum garnet (YAG) by SPS processing

Naum Frage, Sergey Kalabukhov, Nataliya Sverdlov, Vladimir Ezersky, Moshe P. Dariel *

Ben-Gurion University of the Negev, Beer-Sheva, Israel

Received 26 May 2010; received in revised form 29 July 2010; accepted 2 August 2010
Available online 25 August 2010

Abstract

Nano-size YAG powder co-mixed with 0.25 wt.% LiF was used to fabricate transparent polycrystalline YAG specimens by means of the Spark Plasma Sintering (SPS) technique. The presence of the LiF additive in the initial nano-powder allows obtaining fully dense disc shaped (up to 4 mm thick) transparent specimens at the outcome of a 2 h treatment at 1300 °C. The presence of LiF plays a key role in the mass transport related effects during the densification of YAG to full density and also in the elimination of the residual carbon contamination, allowing reaching a level of optical transmittance close to the theoretical value.

Keywords: YAG; SPS; Optical transparency; LiF additive

1. Introduction

Yttrium aluminum garnet (YAG) is an oxide ceramic with outstanding structural and functional properties. It displays excellent high temperature strength and low creep rate and reasonably good mechanical properties.[1] It is well known as a laser gain host crystal and as an excellent IR transparent window material. Initially, YAG was utilized essentially in its single crystal form, over the last decades, however, due to the greatly enhanced availability of high purity powder and advanced processing technologies, polycrystalline YAG has also been manufactured at required quality levels. Since the fabrication costs of polycrystalline YAG are lower than those of single crystals, the increased demand for an adequate supply in the various fields of application has motivated further processing activity. In order to achieve the required optical properties, i.e. transparency, it is imperative to eliminate the presence of pores and of secondary phases, whether those due to impurities or to departure from the stoichiometric composition. This last point is of particular significance, since YAG ($Y_3Al_5O_{12}$) is a stoichiometric compound and any shift from the stoichiometric composition entails the appearance of secondary phases. Polycrystalline YAG prepared by powder technology is less apt than single crystal YAG to undergo catastrophic failure, as cracks that may run freely in single crystals are impeded by the grain boundaries in the polycrystalline ceramic. Powder technology based processing of polycrystalline YAG also lends itself more easily to large size material production.

Most of the reported procedures for the fabrication of polycrystalline YAG are based on the pressureless sintering of the YAG powders manufactured by different methods[2–8] at 1700 °C or higher temperature. High optical quality YAG was obtained by adding SiO_2 as a sintering additive that provides some liquid phase contribution to the full densification of the YAG powder.[9] One of the procedures that has been put forward for the manufacture of a polycrystalline laser material is a multi-stage process that combines cold isostatic pressing (CIP), high temperature vacuum anneal and is completed by hot-isostatic pressing (HIP) in the 1450–1550 °C range for 5 h under 200 MPa argon. This process yields high optical quality transparent YAG with a fine 1–2 μm grain size.[10]

Over the last decade electrical field assisted sintering, also often called Spark Plasma Sintering, (SPS), has gained great popularity as a highly effective approach for consolidating ceramic materials. The SPS technique allows the full densification of ceramics at a lower processing temperature with significantly shorter treatment durations, partly due to the very high heating rates that are attainable. Beside these advantages,

* Corresponding author at: Ben-Gurion University, Materials Engineering, Ben-Gurion Av, Beer-Sheva, Israel. Tel.: +972 8 6461472; fax: +972 8 6477148.
E-mail address: dariel@bgu.ac.il (M.P. Dariel).

0955-2219/$ – see front matter © 2010 Elsevier Ltd. All rights reserved.
doi:10.1016/j.jeurceramsoc.2010.08.006

one serious drawback of SPS processing is linked to the carbon rich atmosphere, in which it is performed. The carbon originates in the graphite die, which is an integral part of the processing unit and serves as a heating element. As a consequence, the SPS processed samples often have a high carbon impurity content, which impairs seriously their optical transparency.[11]

Chaim et al.[12,13] carried out extensive studies on the densification mechanisms of various ceramics by the SPS technology. The authors reported the results of several trials for the fabrication of polycrystalline YAG by SPS processing. Even though relatively high density levels were obtained, the reported optical transparency levels were low, in the 15–20% range, as compared to a theoretical transparency level (close to 90%). The authors attributed the low transparency to the presence of residual pores. They actually concluded that with increasing grain size reached at the peak SPS treatment, the elimination of the residual closed pores was not achievable and that their presence was an inevitable feature of the microstructure resulting from SPS processing. Spark Plasma Sintering has also been employed for the consolidation of lyophilized (dry-freezing) gels but only a relatively low transparency level was obtained.[14]

Recently Frage et al.[15,16] reported the SPS processing parameters for polycrystalline $MgAl_2O_4$, spinel ceramic samples with high transparency close to the theoretical one. The high transparency level was associated with the presence of 1 vol.% of LiF additive, which accelerates the rate of synthesis of spinel from elemental oxide powders, its consolidation to full density and provides a cleansing effect that allows eliminating the carbon impurities. The results of this study also support the findings of by Rozenburg et al.,[17] namely that the presence of the LiF additive promotes the consolidation of the samples.

Considering the successful manufacture of transparent spinel[16], it was of obvious interest to apply a similar manufacturing approach and to verify whether the addition of the LiF additive exerts a positive effect on the densification and on the optical transparency of YAG. The present communication reports on the fabrication of transparent YAG specimens by SPS of commercial nano-size YAG powder and on the effect of the LiF additive.

2. Experimental procedures

Spherical shape (Nanocerox, Inc.) powder with 50 nm average size was used throughout the experiments. Since one of the objectives was to assess the effect of LiF additions, the latter (Alfa Aesar 99,985 pure) was added to some of the powder lots in fractions ranging from 0.25 to 4 wt.%. The addition of LiF to YAG powder at more than 0.25 wt.% leads to the formation of cracks within the samples and eventually to their breaking up. It was consequently decided at an early stage of the study, to focus the research on YAG doped with 0.25 wt.% LiF additive. In order to define the effects of the LiF addition, as precisely as possible, all characterization procedures were performed in parallel on un-doped and LiF-doped powders.

The powder samples were inserted in the 20 mm diameter graphite die of the SPS apparatus (FCT–HP D5/1). Identical parameter profiles were applied to doped and un-doped powders

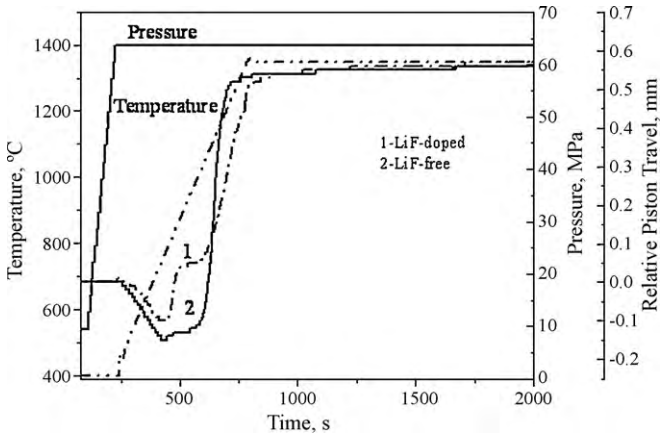

Fig. 1. The temperature and pressure regimes followed in the course of the SPS treatment. Also shown are the punch displacement curves (1 and 2), which reflect the length variation of the samples in the course of the SPS process.

in order to eliminate any perturbing change of the extraneous process parameters. The temperature was measured by a pyrometer focused on the upper graphite punch. It is important to mention that the reported temperatures are the nominal temperatures, as measured in the specific SPS set-up that was used in the present study. The main process parameters used for heating and holding at the sintering temperature as well as the displacement of the upper punch, which reflects the shrinkage, i.e. densification of the sample, are shown in Fig. 1. The highest sintering temperature was 1300 °C. The pressure loading of the samples starts from 3 kN and increases before heating to 20 kN, corresponding to a maximal external pressure of 62 MPa. The holding time for achieving adequate transparency had to be about 2 h.

After the SPS treatment, the relative density of the samples was determined by the liquid displacement method (the theoretical density of YAG was taken as 4.55 g cm^{-3}). The LiF-doped specimens attained full density at the outcome of the SPS process, while the specimens sintered in the absence of the LiF addition had a minor amount (about 0.5 vol.%) of residual porosity. A High Resolution Scanning Electron Microscopy (HRSEM) (JEOL-7400) was used for microstructural characterization of the sintered specimens. In order to reveal the microstructure, the polished YAG samples had to undergo thermal etching under an air atmosphere at 1300 °C for 2 h. The grain size distribution was determined using the SEM pictures and the data analysed with the Thixomet™ image analysis software. Approximately 300 grains were used for each data set. The crystal structure of the as-received powder as well as that of the various samples after SPS treatments was verified by X-ray diffraction (XRD) in a Philips 1050/70 powder diffractometer.

The microstructural characterization included a TEM (JEOL-2010) examination. The YAG specimens were cut into small, 3 mm diameter discs, 0.3 mm thick. The discs were thinned to approximately 0.15 mm thickness by polishing with diamond paste and were bonded to a copper grid with epoxy glue. The disc and its Cu support were flipped over and the same thinning procedure applied until approximately 0.1 mm thickness. The final perforation stage was carried out using a Gatan precision ion polishing system (PIPS™).

The mechanical properties included Vickers hardness testing using a Buehler micro-hardness tester (MMT-7) under a 300 g load. Three point bending tests (ASTM standard C1161) were conducted on 3 mm × 4 mm × 20 mm bars in an LRX Plus LLOYD instrument (Lloyd Instruments). The elastic modulus of the composites was derived from ultrasonic sound velocity measurements. Eighteen samples of doped and un-doped ceramics were tested.

3. Results

3.1. Dimensional changes

Fig. 1 shows the profiles of the parameters (temperature and pressure) that were applied in the course of the SPS consolidation cycle. The dash-dot curve (YAG co-mixed with LiF) and the solid curve standing for the LiF-free sample describe the location of the punch, which follows the thermal expansion and the dimensional changes induced by sintering. According to the recorded data (Fig. 1), the first effect of the sintering induced longitudinal contraction is detectable at approximately 760 °C, for the powder which was co-mixed with LiF. In contrast, such uni-dimensional changes in the un-doped YAG are perceivable only at 900 °C, a significantly higher temperature. The rate of the densification of the doped powder in the temperature range 760–900 °C is significantly higher than that for un-doped specimens. This feature may be attributed to the formation of a small amount of the liquid phase, which promotes the rearrangement of YAG particles and leads to an increased relative density of the samples. Nevertheless, the samples reached the same level of density, namely nearly full density, at the same temperature (1300 °C).

3.2. Optical and SEM microscopy

Micrographs of the fracture surface and of the polished surface that were obtained by HRSEM are shown in (Figs. 2 and 3). The grain size distribution (Fig. 4) of samples that contained the LiF additive and of the LiF-free ones, are shown in Fig. 4a and b. The micrographs put in evidence the difference between these samples. The un-doped specimens display a fine sub-micron microstructure, while the LiF-doped samples have a slightly coarser structure (average particle size of about 1.7 μm). The presence of the residual porosity in the samples fabricated in the absence of LiF is visible in the image of the thermally etched polished sample. In the LiF-doped sample the fracture surface is clearly transgranular, while it is mostly inter-granular in the un-doped YAG sample (Fig. 3a and b).

3.3. TEM

TEM images of the un-doped YAG sample show a rather uniform grain size in the sub-micron range with straight large angle grain boundaries (Fig. 5). A striking feature of these samples is the presence of numerous spherical 10–20 nm diameter occlusions, well embedded in approximately 15–20% of the grains. In some rare instances, non-spherical occlusions were present

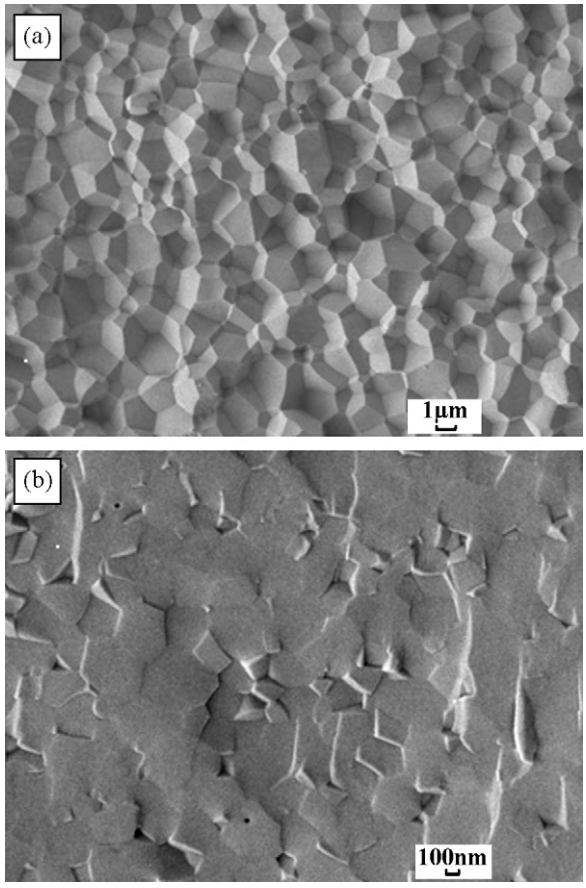

Fig. 2. High resolution SEM images of the fracture surface of: (a) LiF-doped YAG, (b) un-doped YAG specimens.

at the triple junctions of the grain boundaries (Fig. 6). Spherical occlusions are also present in the LiF-doped YAG but at a significantly lower concentration. The presence of amorphous carbon inclusions, as identified by EDS analysis, at triple junctions was also observed (Fig. 7). Such carbon inclusions are frequently encountered in the course of the TEM examination of un-doped samples, in contrast of their quasi-total absence in the LiF-doped ones. A characteristic feature of the LiF-doped and thinned YAG TEM samples was their extreme fragility that caused the grains adjacent to the central perforation hole to break off under their own weight, along the grain boundaries, when placed on the copper grid of the TEM. These grain boundaries coincide with the crystallographic facets, as shown in Fig. 8. Straight boundaries and a grain shape with angles close to 120° attest to a quasi-stable microstructure.

3.4. Mechanical properties

The mechanical properties of the un-doped and doped YAG samples are summarized in Table 1.

3.5. Optical transparence

The optical transparence of the un-doped and doped YAG samples is shown in Fig. 9. This figure puts in clear evidence the dramatic effect of the LiF doping on the optical properties of

Table 1
Mechanical properties of the SPS processed YAG samples (average values of 18 measurements).

Relative density, %, ±0.5	Young modulus, GPa, ±2	Hardness, HV, ±10	Bending strength, MPa, ±15
100[a], 99.5	290[a], 290	1450[a], 1490	300[a], 340

[a] Doped specimens.

the SPS processed YAG specimens. Whereas the transparence of the doped samples is close to the theoretical values, that of the un-doped samples hovers in the 50–60% in the IR part of the spectrum with even lower values in the optical range.

4. Discussion

The main goal of the present study was to verify that the presence of the LiF additive in SPS processed YAG powder allowed obtaining transparent samples, similar to the results that had been observed with SPS processed spinel. The results clearly and unambiguously underscore a positive answer to these expectations. The addition of LiF indeed yields fully dense and highly transparent samples after relatively short SPS treatments at 1300 °C. In a previous paper[15] that treated the processing of spinel samples, the transparency was attributed to the cleansing effect of the LiF additive, which by reaction with the carbon contaminant gave rise to volatile $(CF)_n$ species that were driven off in the course of the SPS cycle, as long as an open network of channels was maintained. Excess Li released from the additive is incorporated in the ceramic YAG matrix, substitutes for the higher positive valence Y and/or Al cations and, as a result of charge equilibrium requirements, generates oxygen vacancies as shown, using the Kroger–Vink notation, in Eqs. (1) and (2):

$$nC + n\mathrm{LiF} \rightarrow n\mathrm{Li}''_{\mathrm{Y(Al)}} + nV_{\mathrm{O}}^{**} + (\mathrm{CF})_n \uparrow \quad (1)$$

$$2\mathrm{LiF} \rightarrow 2\mathrm{Li}''_{\mathrm{Y(Al)}} + 2\mathrm{F}_{\mathrm{O}}^{*} + V_{\mathrm{O}}^{**} \quad (2)$$

Oxygen is the slowest diffusing species in YAG[17] and determines the mass transport properties of the latter. Oxygen diffuses by a vacancy mechanism and, consequently, excess oxygen vacancies enhance its diffusivity and, similar to the effect observed in spinel, accelerates grain growth.[16] Indeed as shown in Fig. 4, the average grain size of the LiF-doped YAG is larger than that of the un-doped one.

An interesting and to some extent puzzling feature was the presence of numerous perfectly spherical occlusions in un-doped YAG and their almost complete absence in the LiF-doped matrix. One is led to conclude that the presence of the LiF opened the route for the elimination of the occluded species, most likely residual gas entrapped when the moving grain boundaries swept over triple point junctions such as shown in Fig. 6. At elevated

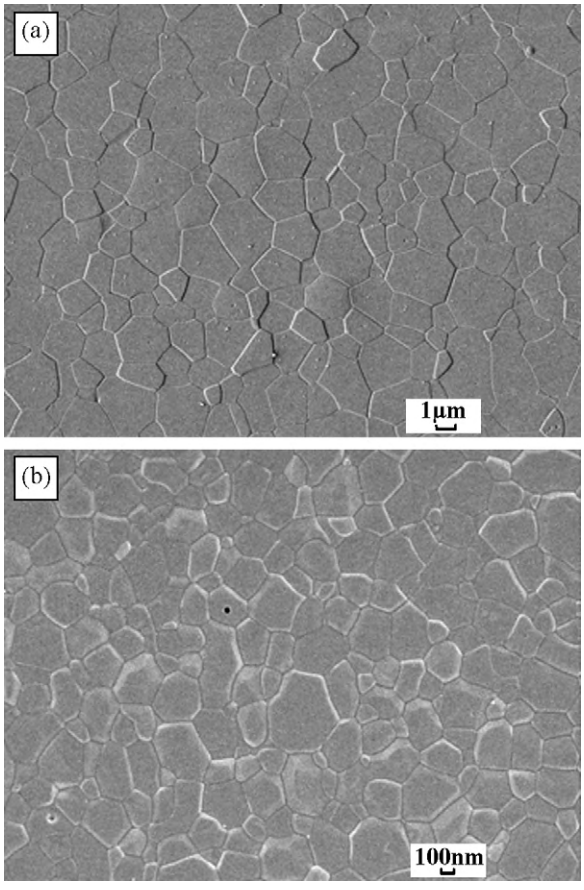

Fig. 3. High resolution SEM pictures of the polished and thermally etched surface of: (a) LiF-doped YAG sample; (b) un-doped YAG sample.

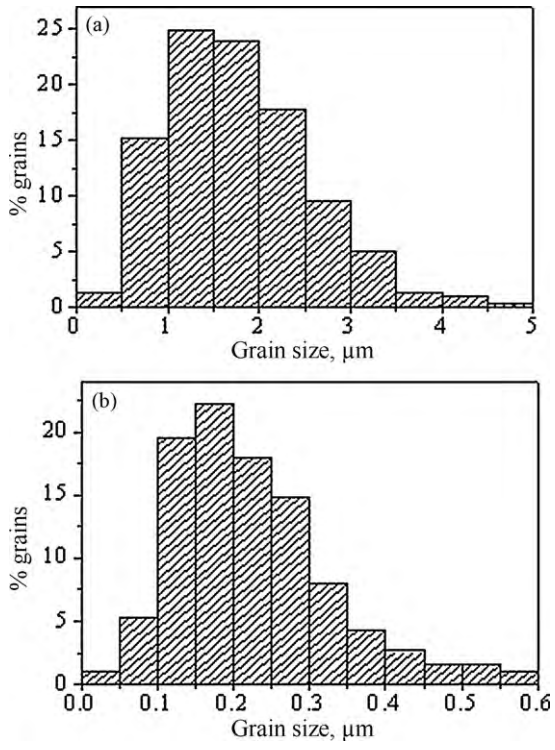

Fig. 4. Grain size distribution of samples similar to those shown in Fig. 3. (a) LiF-doped YAG; (b) un-doped YAG.

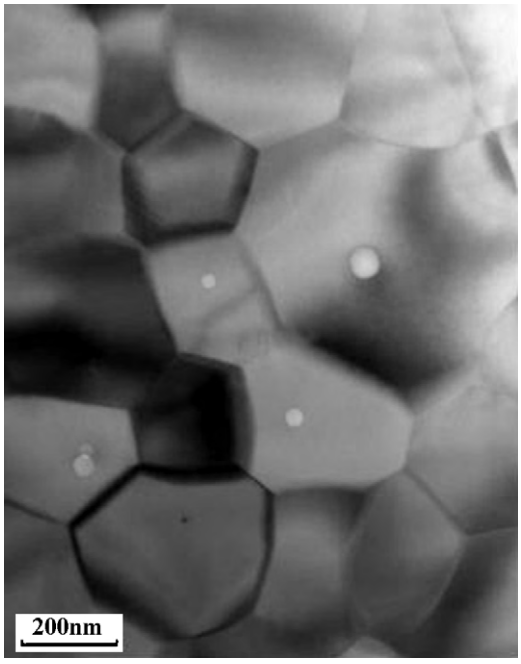

Fig. 5. TEM image of the SPS processed, un-doped YAG sample. Notice the relatively stable sub-micron structure and notice the spherical occlusions that are present in several grains. Notice also at the lower left of the picture two superposed occlusions located at different depths of the foil.

temperature, the surface minimization trend caused the volume of the entrapped gas to adopt a perfect spherical shape. High temperature wetting experiment by the sessile drop method has shown near zero contact angle of molten LiF on the spinel surface indicating a perfect wetting behavior[16]. It is not unlikely that a similar situation prevails on a YAG surface. Perfect wetting implies the presence of thin inter-granular surface layers in the YAG matrix that provides the escape channels of the entrapped gas. In the absence of such escape routes in the un-doped YAG,

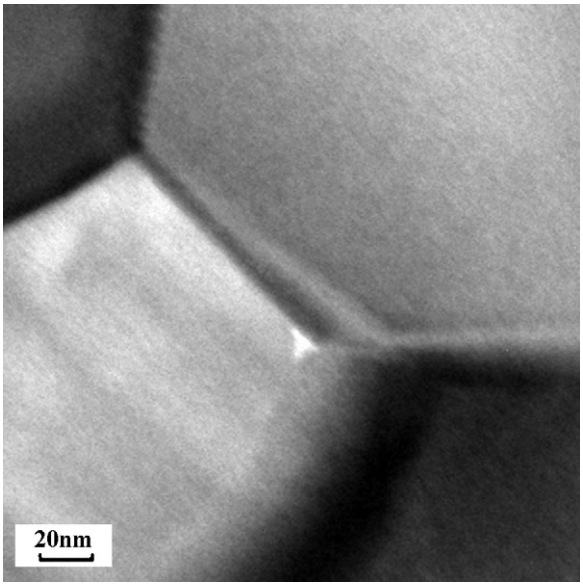

Fig. 6. The TEM image of a residual void at the triple junction of grain boundaries.

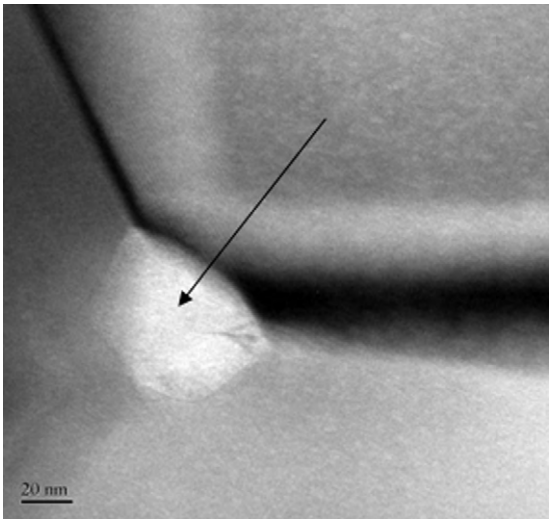

Fig. 7. TEM image of an amorphous carbon inclusion trapped at the triple junction of the YAG structure.

any residual gas stays entrapped in spherical occlusions. At the present of our understanding this mechanism is a tentative one and requires positive validation.

In addition to the incorporation of Li^+ into the ceramic matrix, the F^- anions scavenge the carbon contamination and act as cleansing agents by combining with carbon to generate volatile fluoro-carbon species that are driven off during the high temperature treatment, as long as an open channel network is still available. This latest requirement determines the profile of the pressure application regime in the course of the SPS treatment.

The residual concentration of the doping species Li and F in the YAG lattice is as yet an unresolved issue. We have reported in a previous work on the use of the SPS technique for the fabrication of highly transparent spinel[16], using an approach similar to that described above for transparent YAG. Efforts were made in order to determine the concentration of the residual dopant concentration in the SPS fabricated spinel. We report herewith the results because they represent very likely results that would have been found in the YAG samples. Polished spinel specimens, LiF-doped and un-doped, were examined by ToF-SIMS analysis, using a ION-TOF IV instrument installed at the M2B2 research unit of the Fondazione Bruno Kessler (FBK) in Trento, Italy. The analyses were run using a Ga^+ 15 keV beam in bunched mode to maximize mass resolution. The doped spinel samples had a LiF additions at a level similar to that employed in the YAG samples. Semi-quantitative depth profiling results were obtained from a sub-micron surface depth range. The analysis was run on positive and negative polarity to follow the signals of, respectively, the metals (Li as additive, Mg and Al as matrix) and C and F. The profile based on the signals in positive polarity showed a constant content of the matrix species (such as Mg and Al). When considering the LiF-doped spinel samples, the dopant (LiF) signal (Li^+) also showed a constant content in the examined layer, suggesting a homogenous distribution of the Li species in the SPS treated pellet. In contrast, the Li^+ signal was basically absent in the un-doped sample.

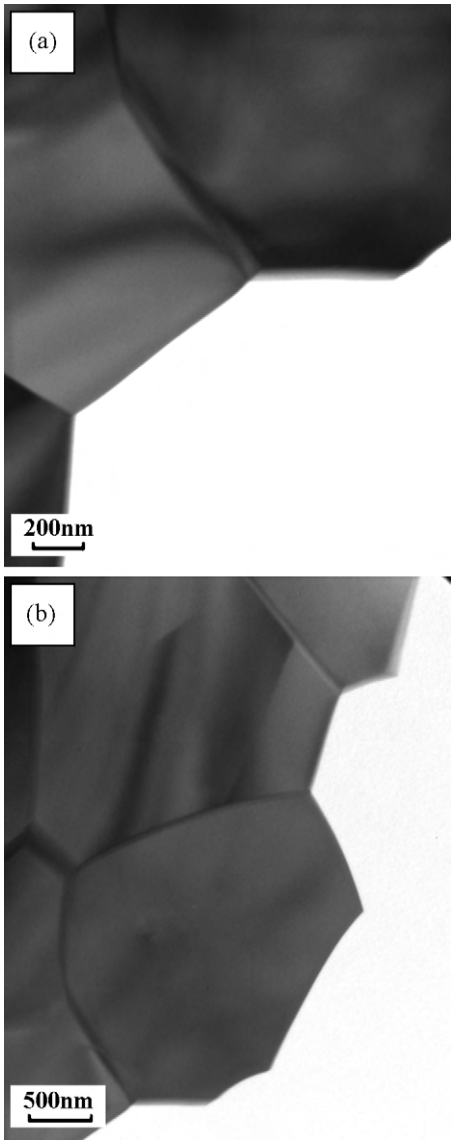

Fig. 8. The edges of the perforation hole in the thinned LiF-doped YAG TEM sample. Notice the edges of the hole, which coincide with grain boundaries, suggesting that the boundaries were weakened most likely by the presence of thin LiF grain-boundary layers. The grains adjacent to the weakened boundaries broke off during the thinning process.

With regard to the data obtained in negative polarity, the F signal was intense in the LiF-doped samples, whilst it disappeared in the background noise in the un-doped sample. These results obtained in the SPS treated oxide samples suggest that the major fraction of the LiF additive is retained in the samples after the SPS treatment. The Li component is most likely incorporated in the matrix as a cation substitute while the F anion substitutes for oxygen. Charge equilibrium is maintained by adjusting the concentration of oxygen vacancies, a mechanism that supports the enhanced mass transport effects observed in the LiF-doped samples.

The Young's modulus of the doped and doped specimens display quasi-identical values, the values of Vicker's hardness and of the bending strength of un-doped specimens is slightly higher then for LiF-doped samples. These differences reflect the

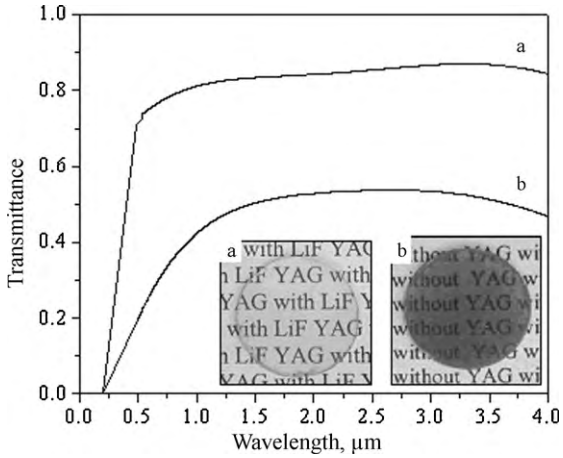

Fig. 9. Optical transmittance of YAG specimens (a) with and (b) without LiF addition. Inserts: the SPS processed samples specimens, 2 mm thick.

microstructural and fracture mode dissimilarity. The mechanical properties of the SPS processed YAG are in a good agreement with those reported by Mezeix and Green[1] for YAG single crystal ceramic.

The lack of transparence in the un-doped YAG samples is attributed to its higher pore concentration as indicated in TEM Figs. 5 and 6 and to the presence of residual carbon contamination, an example of which is shown in Fig. 7.

5. Summary

The addition of 0.25 wt.% LiF to nano-sized YAG powder allows obtaining transparent YAG, up to 5 mm thick discs, by SPS processing. Fully dense powders are obtained after a 2 h long hold time at 1300 °C under a pressure of 80 MPa. The mechanical properties of the SPS processed YAG specimens are on par with those of samples prepared by conventional consolidation techniques. The addition of the LiF additive promotes sufficient transparency, but also remarkable grain growth. The final average grain size of the LiF-doped initially nano-sized YAG powder was of the order of 1.7 μm.

Acknowledgements

Supported partly by the Israel Ministry of Science, under Grant No. 3-3429. We wish to express our thanks and appreciation to the FBK – Fondazione Bruno Kessler at Trento, Italy for enabling us to carry out high resolution microstructural identification and, in particular to Dr. Salvatore Gennaro who performed the TOF measurements and analysed the results.

References

1. Mezeix L, Green D. Comparison of the mechanical properties of single crystal and polycrystalline yttrium aluminum garnet. *Int J Appl Ceram Technol* 2006;**3**:166–76.
2. Wen L, Sun X, Xiu Z, Chen S, Tsai CT. Synthesis of nanocrystalline yttria powder and fabrication of transparent YAG ceramics. *J Eur Ceram Soc* 2004;**24**:2681–8.

3. Li X, Li Q, Wang J, Yang S, Liu H. Synthesis of Nd^{3+} doped nanocrystalline yttrium aluminum garnet (YAG) powders leading to transparent ceramic. *Opt Mater* 2007;**29**:528–31.
4. Rabinovitch Y, Bogicevic C, Karolak K, Tetard D, Dammak D. Freeze-dried nanometric neodymium-doped YAG powders for transparent ceramics. *J Mater Process Technol* 2008;**199**:314–20.
5. Chen ZH, Li JT, Xu JJ. Fabrication of high transparent YAG ceramics by vacuum sintering at low temperature. *Key Eng Mater* 2008;**368–372**:420–2.
6. Appiagyei KA, Messing GL, Dumm JQ. Aqueous slip casting of transparent yttrium aluminum garnet (YAG) ceramics. *Ceram Int* 2008;**34**:1309–13.
7. Chen ZH, Li JT, Xu JJ, Hu ZG. Fabrication of YAG transparent ceramics by two-step sintering. *Ceram Int* 2008;**34**:1709–12.
8. Wang J, Zheng S, Zeng R, Dou S, Sun Z. Microwave synthesis of homogeneous YAG nanopowder leading to a transparent ceramic. *J Am Ceram Soc* 2009;**92**:1217–23.
9. Maitre A, Salle C, Boulesteix R, Baumard J-F, Rabinovitch J. Effect of silica on the reaction sintering of polycrystalline Nd:YAG ceramics. *J Am Ceram Soc* 2008;**91**:406–13.
10. Lee HD, Mah TI, Partasarathy TA, Low-Cost Processing of Fine Grained Transparent Yttrium Aluminum Garnet, in *8th Int Conf Adv Ceram Comp A: Ceram Eng Sci Proc* 2008;**25**(3)147–52.
11. Bernard-Granger G, Benameur N, Guizard C, Nygren M. Influence of graphite contamination on the optical properties of transparent spinel obtained by spark plasma sintering. *Scripta Mater* 2009;**60**:164–7.
12. Chaim R, Marder-Jaeckel R, Shen JZ. Transparent YAG ceramics by surface softening of nanoparticles in spark plasma sintering. *Mater Sci Eng A* 2006;**429**:74–8.
13. Chaim R, Kalina K, Shen Z. Transparent yttrium aluminum garnet (YAG) ceramics by spark plasma sintering. *J Eur Ceram Soc* 2007;**27**: 3331–7.
14. Suarez M, Fernandez A, Menendez JL, Nygren M, Torrecillas R, Zhao Z. Hot isostatic pressing of optically active Nd:YAG powders doped by a colloidal processing route. *J Eur Ceram Soc* 2010;**30**:1489.
15. Frage N, Cohen S, Meir S, Kalabukhov S, Dariel MP. Spark pasma sintering (SPS) of transparent magnesium–aluminate spinel. *J Mater Sci* 2007;**42**:3273–5.
16. Meir S, Kalabukhov S, Froumin N, Dariel MP, Frage N. Synthesis and densification of transparent magnesium aluminate spinel by SPS processing. *J Am Ceram Soc* 2009;**92**:358–64.
17. Rozenburg K, Reimanis IE, Kleebe H-J, Cook RL. Chemical interaction between LiF and $MgAl_2O_4$ spinel during sintering. *J Am Ceram Soc* 2007;**90**:2038–42.